J. Fluid Mech. (1977) *vol.* 80, *part* 1, *pp.* 1–15
Printed in Great Britain

Asymmetric two-dimensional jet efflux from a channel

By C. SAMUEL MARTIN
School of Civil Engineering, Georgia Institute of Technology, Atlanta

(Received 10 May 1976)

Irrotational flow of two-dimensional jets from a channel is treated without direct use of a logarithmic hodograph plane. An analytical approach is introduced for solving the general problem of two jets issuing from a channel with three end plates. Numerical values of the contraction coefficient and the angle of jet deflexion are obtained for the special case where the two jets are located symmetrically and all the end plates are in line. Limiting cases of the resulting single-jet problem are the symmetric and asymmetric configurations solved by von Mises. Results for the asymmetric case improve upon the theoretical values reported by von Mises, and compare favourably with existing experimental data.

1. Introduction

The efflux of a two-dimensional jet from a slot in a channel has been treated for various configurations by a number of investigators for over a century. Single-jet problems over plane and curved boundaries with or without gravity arise in numerous practical situations, as reported by Robertson (1965). The two-jet investigation included in the present paper was initiated because of interest in jet and cavity flows and jet configurations in fluid amplifiers and orifice-plate valves. The use of finite-difference and finite-element techniques in the last two decades has meant a lessening in the application and development of classical conformal-mapping techniques to potential-flow problems. Instead of the usual mapping of the logarithmic hodograph plane, the present paper introduces a technique that reduces the problem to the solution of a boundary-value problem in a rectangle. Although somewhat similar techniques have been employed by Thom & Apelt (1961), Cassidy (1965), Markland (1965) and Strekloff & Moayeri (1970), the current method can be readily extended to gravity-free flows past curved boundaries (Martin 1967).

The asymmetric two-jet efflux problem shown in figure 1 is solved by applying the solution technique described below. Only a limited number of problems of two jets issuing from channels have been solved completely. Typically, the end plates BC and IJ are eliminated and the plate EG aligned normal to the flow (Birkhoff & Zarantonello 1957; Robertson 1965). The simpler single-jet problem with two end plates lined up was formulated in the last century by Michell (1890). Further discussion of the problem without plate alignment can be found in Ciscotti (1908, 1914) and Greenhilll (1910). In none of these instances were the resulting elliptic integrals evaluated. Von Mises (1917) treated special cases of

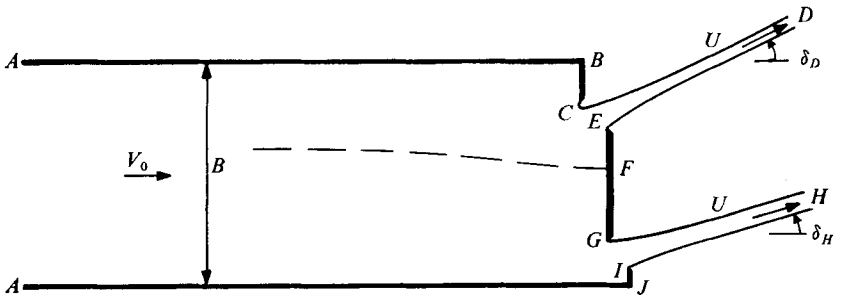

FIGURE 1. Definition sketch of physical plane.

the more general single-jet problem discussed by Ciscotti, namely (i) a single symmetric jet and (ii) an asymmetric jet with one end plate absent and the other end plate in line with the end of the opposite channel wall.

As are most if not all conformal-mapping solution techniques for complex asymmetrical multiple-jet and multiple-plate free-streamline problems (Robertson 1965; Birkhoff & Zarantonello 1957), the method presented here is an implicit or inverse one for which the exact location of the solid boundaries cannot be prescribed initially. This difficulty can be resolved by parametric studies of the relationships between quantities that can be prescribed and the resulting physical dimensions. If necessary, iterative numerical schemes may be employed.

Although the solution is demonstrated to be valid for a general two-jet efflux, parametric curves are presented only for the case in which the two jets are symmetric relative to each other and the end plates are in line. The limiting forms of this configuration are the two cases cited above that von Mises (1917) solved. Separate simple solutions are effected for the two limiting cases (i) to provide a check and comparison for the more general solution and (ii) to improve the accuracy of the values reported by von Mises for the asymmetric jet.

2. Conformal transformation

The general two-dimensional flow problem that we pose here is shown in the physical plane in figure 1. We assume steady irrotational flow of an incompressible fluid from the two openings, which are in general not lined up with the two lips BC and IJ or the middle plate EG. The special case in which all three plates are lined up and the two jets are symmetric can be further reduced to the two-lip symmetric and the single-lip asymmetric single-jet problems solved by von Mises.

The boundary-value technique applied here has already been used for free-streamline flows with curved boundaries (Martin 1967). Basically, we use the fact that, through conformal transformations of analytic functions, any two of the various conjugate harmonic functions satisfy Laplace's equation. The boundary-value problem can be posed, then, in any conformal plane in terms of any two conveniently selected analytic functions.

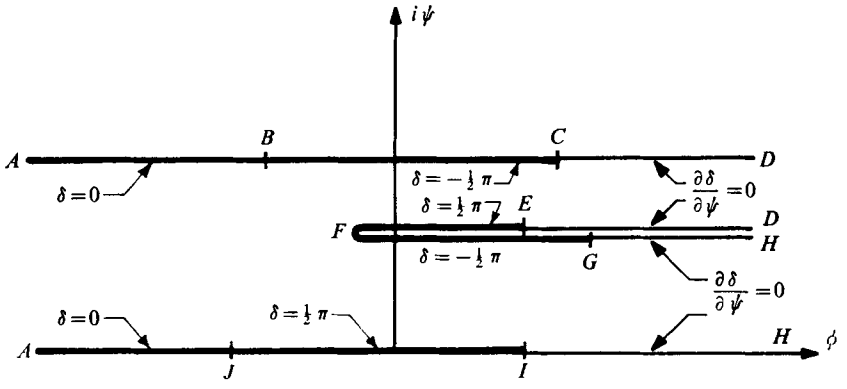

FIGURE 2. Boundary-value problem in complex-potential plane.

For the two-jet problem depicted in figure 1 the physical plane is defined by $z = x + iy$. We let ϕ be the velocity potential and ψ be the stream function, for which the complex potential $w = \phi + i\psi$, as shown in figure 2. We express the complex (conjugate) velocity potential ζ in the form

$$\zeta = \frac{1}{U}\frac{dw}{dz} = \frac{u}{U} - i\frac{v}{U} = \frac{V}{U}e^{-i\delta}, \tag{1}$$

where δ is the angle of the velocity vector relative to the horizontal, u and v are the x and y components of the velocity vector $\mathbf{V}$, and U is the jet velocity shown in figure 1. Even though the hodograph and logarithmic hodograph planes are not mapped in applying the technique described here the logarithmic hodograph variable Ω is crucial to the solution. The complex function

$$\Omega = \ln\zeta = \ln(V/U) - i\delta \tag{2}$$

is analytic if only the single-valued part of the ln function is used. It follows then that

$$\nabla^2\delta = \partial^2\delta/\partial x^2 + \partial^2\delta/\partial y^2 = 0 \tag{3a}$$

and

$$\nabla^2\left\{\ln\frac{V}{U}\right\} = \frac{\partial^2\{\ln(V/U)\}}{\partial x^2} + \frac{\partial^2\{\ln(V/U)\}}{\partial y^2} = 0. \tag{3b}$$

Equations (3) actually constitute a boundary-value problem for δ and $\ln(V/U)$ in the z plane. Inasmuch as the location of the free streamlines is not known *a priori*, the problem is not simplified however. As the w plane is comprised of straight lines, a more suitable approach would be to solve

$$\partial^2\delta/\partial\phi^2 + \partial^2\delta/\partial\psi^2 = 0 \tag{4a}$$

and

$$\frac{\partial^2[\ln(V/U)]}{\partial\phi^2} + \frac{\partial^2[\ln(V/U)]}{\partial\psi^2} = 0. \tag{4b}$$

For the w plane the boundary-value problem is more easily formulated in terms of δ than in terms of $\ln(V/U)$. On all solid boundaries δ is a constant, as shown in

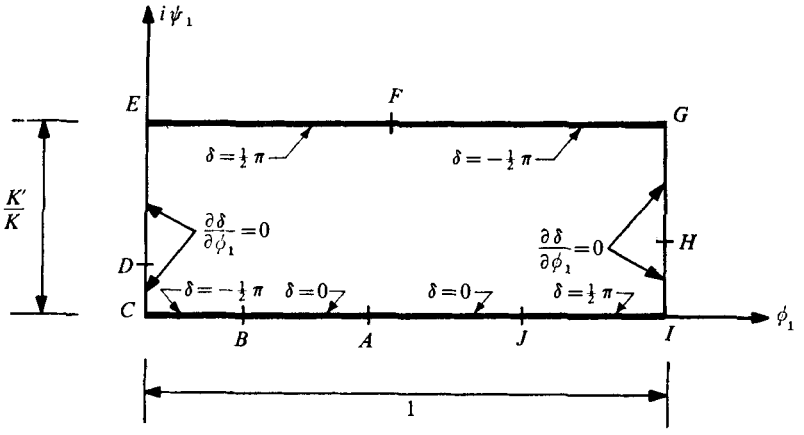

FIGURE 3. Boundary-value problem in rectangular w_1 plane.

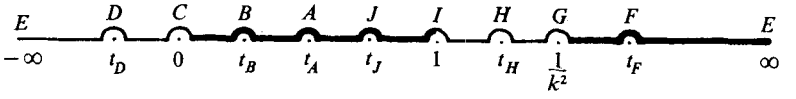

FIGURE 4. t plane.

figure 1 for the lines AB, BC, EF, FG, IJ and AJ. The Cauchy–Riemann conditions relating δ and $\ln(V/U)$ in the w plane are

$$\frac{\partial\delta}{\partial\psi} = \frac{\partial\{\ln(V/U)\}}{\partial\phi}, \quad \frac{\partial\delta}{\partial\phi} = -\frac{\partial\{\ln(V/U)\}}{\partial\psi}. \tag{5a,b}$$

The boundary condition on the free streamlines in the absence of gravity is $V = U$ or $\ln(V/U) = 0$, for which the normal gradient of δ is zero in the z plane, i.e. $\partial\delta/\partial n = 0$. This boundary condition transforms in the w plane to $\partial\delta/\partial\psi = 0$ upon application of (5a). The boundary-value problem shown in figure 2 is still somewhat ill posed as on the lines DEF and FGH both Dirichlet and Neumann boundary conditions are specified. This problem of a combination of an inhomogeneous Dirichlet boundary condition and a homogeneous Neumann boundary condition on the same straight line can be alleviated, however, by transforming the entire boundary-value problem in the w plane to a rectangle in another plane.

The complex plane that comprises the rectangle is defined by

$$w_1 = \phi_1 + i\psi_1. \tag{6}$$

If w_1 is an analytic function the boundary-value problem is a solution to

$$\partial^2\delta/\partial\phi_1^2 + \partial^2\delta/\partial\psi_1^2 = 0 \tag{7a}$$

and

$$\frac{\partial^2\{\ln(V/U)\}}{\partial\phi_1^2} + \frac{\partial^2\{\ln(V/U)\}}{\partial\psi_1^2} = 0. \tag{7b}$$

For the transformed boundary-value problem shown in figure 3, we employ the Schwarz–Christoffel theorem to relate the w and w_1 planes through an intermediate plane, the t plane. The t plane, shown in figure 4, has the points C, I and E fixed at 0, 1 and infinity respectively. All the remaining points except G can have assigned values. If the value t_G of t at G is taken as $1/k^2$, where k is the modulus of the Jacobian elliptic functions, the t plane can be mapped into the w_1 plane (Byrd & Friedman 1954, p. 17) by

$$w_1 = K^{-1}\,\mathrm{sn}^{-1}[t]^{\frac{1}{2}}, \tag{8}$$

where K is the elliptic integral of the first kind and sn is the sine-amplitude Jacobi function. The inverse relationship is

$$t = \mathrm{sn}^2[Kw_1, k] = \mathrm{sn}^2[Kw_1]. \tag{9}$$

The ratio of the lengths of the sides of the rectangle, imaginary to real, is K'/K, where K' is the complementary integral of the first kind. For the w_1 plane shown in figure 3, however, $\phi_{1I} = 1$ and $\psi_1 = K'/K$ on EFG. The location of each of the remaining six points in the t plane is determined by the relative positions of A, B, D, F, H and J in the w_1 plane. The relationships are

$$t_A = \frac{1}{k}\frac{H^2[K\phi_{1A}]}{\Theta^2[K\phi_{1A}]}, \quad t_B = \frac{1}{k}\frac{H^2[K\phi_{1B}]}{\Theta^2[K\phi_{1B}]}, \quad t_D = \frac{1}{k}\frac{H^2[iK\psi_{1D}]}{\Theta^2[iK\psi_{1D}]}, \tag{10a–c}$$

$$t_F = \frac{1}{k}\frac{\Theta^2[K\phi_{1F}]}{H^2[K\phi_{1F}]}, \quad t_H = \frac{1}{k}\frac{H^2[K+iK\psi_{1H}]}{\Theta^2[K+iK\psi_{1H}]}, \quad t_J = \frac{1}{k}\frac{H^2[K\phi_{1J}]}{\Theta^2[K\phi_{1J}]}, \tag{10d–f}$$

where H and Θ are theta functions, which were employed because of their quick rate of convergence in the particular series expansions defined in the appendix.

The w plane is related to the t plane by

$$\frac{dw}{dt} = \frac{V_0 B}{\pi}\frac{(t_A - t_D)(t_H - t_A)(t - t_F)}{(t_F - t_A)(t - t_A)(t - t_D)(t - t_H)}, \tag{11}$$

where B is the channel width and V_0 the approach velocity in the channel, as shown in figure 1.

The boundary conditions shown in figure 3 for δ are no longer combined Dirichlet and Neumann conditions on the same straight line, as δ is specified on the two real sides and its normal gradient is known on the other two sides. On the channel sides AB and AJ, $\delta = 0$. The upward flow on the surfaces JI and FE requires $\delta = \frac{1}{2}\pi$, while on BC and FG, $\delta = -\frac{1}{2}\pi$. There exists, of course, a discontinuity in δ at the stagnation point F. On the free streamline surfaces CDE and GHI the transformed boundary condition $\ln(V/U) = 0$ yields $\partial\delta/\partial\phi_1 = 0$. The boundary-value problem delineated in figure 3 is well posed, allowing use of separation of variables and the theory of Fourier series. We first obtain δ as a function of ϕ_1 and ψ_1 from the solution to (7a), and then apply the Cauchy–Riemann conditions to determine $\ln(V/U)$. The complex solution for Ω in terms of δ and $\ln(V/U)$ is

$$\Omega = \Omega(w_1) = \ln(V/U) - i\delta. \tag{12}$$

From (1) and (2) the final physical-plane relationship is

$$dz = \frac{1}{U} e^{-\Omega} \frac{dw}{dw_1} dw_1. \tag{13}$$

The particular physical configuration is obtained from (13), in which Ω is obtained from the boundary-value solution and dw/dw_1 from the conformal-mapping relationships (8) and (11).

3. Boundary-value problem

From separation of variables

$$\delta = \begin{cases} (a_1 \sinh \lambda\psi_1 + a_2 \cosh \lambda\psi_1)(a_3 \sin \lambda\phi_1 + a_4 \cos \lambda\phi_1), & \lambda \neq 0, \quad (14) \\ (b_1\psi_1 + b_2)(b_3\phi_1 + b_4), & \lambda = 0. \quad (15) \end{cases}$$

In the latter case the condition $\partial\delta/\partial\phi_1 = 0$ on GHI yields $b_3 = 0$. The product $b_1 b_4$ must also vanish in order that $\ln(V/U) = 0$ on this line, resulting in $b_1 = 0$ and

$$\delta = A_0, \quad \lambda = 0, \tag{16}$$

where

$$A_0 = \int_0^1 \delta_{CI}(\phi_1)\, d\phi_1 = \int_0^1 \delta_{EG}(\phi_1)\, d\phi_1. \tag{17}$$

Integrating gives

$$A_0 = \tfrac{1}{2}\pi(1 - \phi_{1B} - \phi_{1J}) = \pi\phi_{1F} - \tfrac{1}{2}\pi, \tag{18}$$

or

$$\phi_{1F} = 1 - \tfrac{1}{2}(\phi_{1B} + \phi_{1J}). \tag{19}$$

The boundary condition $\partial\delta/\partial\phi_1 = 0$ on CDE and GHI yields $a_3 = 0$ and $\sin \lambda\phi_{1I} = 0$, from which $\lambda = n\pi$, $n = 1, 2, 3, \ldots$. We express the solution in terms of Fourier series:

$$\delta = A_0 + \sum_{n=1}^{\infty} [A_n' \sinh n\pi\psi_1 + B_n' \cosh n\pi\psi_1] \cos n\pi\phi_1 \tag{20}$$

or, more conveniently,

$$\delta = A_0 + \sum_{n=1}^{\infty} A_n \sinh [n\pi(\psi_{1E} - \psi_1)] \cos n\pi\phi_1 + \sum_{n=1}^{\infty} B_n \sinh n\pi\psi_1 \cos n\pi\phi_1. \tag{21}$$

As a result of satisfying boundary conditions on CI and EG

$$A_n \sinh n\pi\psi_{1E} = 2\int_0^1 \delta_{CI}(\phi_1) \cos n\pi\phi_1\, d\phi_1 = -\frac{1}{n}(\sin n\pi\phi_{1B} + \sin n\pi\phi_{1J}) \tag{22a}$$

and

$$B_n \sinh n\pi\psi_{1E} = 2\int_0^1 \delta_{EG}(\phi_1) \cos n\pi\phi_1\, d\phi_1 = \frac{2}{n} \sin n\pi\phi_{1F}. \tag{22b}$$

The solution for the harmonic conjugate $\ln(V/U)$ is determined by inspection to be

$$\ln \frac{V}{U} = \sum_{n=1}^{\infty} A_n \cosh n\pi(\psi_{1E} - \psi_1) \sin n\pi\phi_1 - \sum_{n=1}^{\infty} B_n \cosh n\pi\psi_1 \sin n\pi\phi_1. \tag{23}$$

The logarithmic hodograph variable Ω can be expressed in terms of elliptic functions as Jacobi's *nome*

$$q = \exp[-\pi(K'/K)], \tag{24}$$

from which

$$\sinh\left[n\pi(K'/K)\right] = \tfrac{1}{2}[q^{-n} - q^{n}]. \tag{25}$$

In terms of q the solution for Ω is

$$\Omega = -\frac{\pi}{2}[1-\phi_{1B}-\phi_{1J}]\,i - 2\sum_{n=1}^{\infty}\frac{q^n(\sin n\pi\phi_{1B}+\sin n\pi\phi_{1J})\sin n\pi(w_1-i\psi_{1E})}{n(1-q^{2n})} - 4\sum_{n=1}^{\infty}\frac{q^n\sin n\pi\phi_{1F}\sin n\pi w_1}{n(1-q^{2n})}. \tag{26}$$

We use Jacobi's (1881) formula relating the incomplete elliptic integral of the third kind Π, the Jacobian zeta function Z and the theta function Θ:

$$\Pi\left[\frac{2Ku}{\pi},\frac{2KA}{\pi}\right] - \frac{2Ku}{\pi}Z\left(\frac{2KA}{\pi}\right) = -2\sum_{n=1}^{\infty}\frac{q^n\sin 2nA\sin 2nu}{n(1-q^{2n})} = \tfrac{1}{2}\ln\frac{\Theta(2Ku/\pi-2KA/\pi)}{\Theta(2Ku/\pi+2KA/\pi)}. \tag{27}$$

The final solution for Ω is

$$\Omega = \frac{\pi}{-2}(1-\phi_{1B}-\phi_{1J})\,i + \tfrac{1}{2}\ln\left[\frac{\Theta[K(w_1-i\psi_{1E})-K\phi_{1B}]\,\Theta[K(w_1-i\psi_{1E})-K\phi_{1J}]}{\Theta[K(w_1-i\psi_{1E})+K\phi_{1B}]\,\Theta[K(w_1-i\psi_{1E})+K\phi_{1J}]}\right] + \ln\frac{\Theta[Kw_1-K\phi_{1F}]}{\Theta[Kw_1+K\phi_{1F}]}. \tag{28}$$

From (8) and (11)

$$\frac{dw}{dw_1} = \frac{2K}{\pi}V_0B\frac{(t_A-t_D)(t_H-t_A)}{t_F-t_A}\frac{[\mathrm{sn}^2(Kw_1)-t_F]\,\mathrm{sn}(Kw_1)\,\mathrm{cn}(Kw_1)\,\mathrm{dn}(Kw_1)}{[\mathrm{sn}^2(Kw_1)-t_A][\mathrm{sn}^2(Kw_1)-t_D][\mathrm{sn}^2(Kw_1)-t_H]}. \tag{29}$$

We use the identities in the appendix relating the Jacobian elliptic functions in (29) and the eta and theta functions, resulting in

$$\frac{dw}{dw_1} = 2\frac{K}{\pi}kk'\frac{(t_A-t_D)(t_H-t_A)}{t_F-t_A}V_0BF_1(Kw_1)\,F_2(Kw_1)\,F_3(Kw_1), \tag{30}$$

where

$$F_1(Kw_1) = \frac{H^2(Kw_1)-t_Fk\Theta^2(Kw_1)}{H^2(Kw_1)-t_Ak\Theta^2(Kw_1)}, \tag{31}$$

$$F_2(Kw_1) = \frac{\Theta(Kw_1)\,\Theta_1(Kw_1)}{H^2(Kw_1)-t_Hk\Theta^2(Kw_1)}, \tag{32}$$

and

$$F_3(Kw_1) = \frac{H(Kw_1)\,H_1(Kw_1)}{H^2(Kw_1)-t_Dk\Theta^2(Kw_1)}. \tag{33}$$

The solution for z, from (13), is

$$d\left(\frac{z}{B}\right) = \frac{2}{\pi}Kkk'\frac{(t_A-t_D)(t_H-t_A)}{t_F-t_A}\frac{V_0}{U}F_1(Kw_1)\,F_2(Kw_1)\,F_3(Kw_1)\,F_4(Kw_1)\,F_5(Kw_1) \times\exp\left[i\pi(\phi_{1F}-\tfrac{1}{2})\right]dw_1, \tag{34}$$

where

$$F_4(Kw_1) = \left[\frac{\Theta[K(w_1+\phi_{1B}-i\psi_{1E})]\,\Theta[K(w_1+\phi_{1J}-i\psi_{1E})]}{\Theta[K(w_1-\phi_{1B}-i\psi_{1E})]\,\Theta[K(w_1-\phi_{1J}-i\psi_{1E})]}\right]^{\frac{1}{2}} \tag{35}$$

and

$$F_5(Kw_1) = \Theta[K(w_1+\phi_{1F})]/\Theta[K(w_1-\phi_{1F})]. \tag{36}$$

4. General solution

A complete geometric description of the boundaries in figure 1 is given by five y dimensions and two x dimensions, resulting in six dimensionless length ratios, usually in terms of the channel width B. Correspondingly, for a given value of k^2 there are six arbitrary values of t, i.e. the positions of the associated points in the w_1 plane. Point F is not completely arbitrary, however, as (19) must be satisfied.

For given values of k^2, ϕ_{1A}, ϕ_{1B}, ϕ_{1J}, ψ_{1D} and ψ_{1H}, we determine the shape of the physical plane by numerical integration of (34). The use of a rapidly converging Fourier series expansion of the eta and theta functions (Byrd & Friedman 1954, p. 314) greatly expedites the calculation. These series expansions are provided in the appendix. An eighth-order integration rule (Abramowitz & Stegun 1964, p. 886) was employed for the numerical integration. The use of complex utility computer routines facilitated the resolution of the integrand of (34) into real and imaginary components.

Special provisions were made in the integration near or around the singularities at points B, F and J. The right-angle stagnation points B and J yield infinite values in the integrand. It can be demonstrated, however, that, in the limit as B is approached from A or C, the integrand varies as $\Delta\phi_1^{-\frac{1}{2}}$, where $\Delta\phi_1$ is the distance away from B. Near point J an identical relationship exists. Equation (34) is integrated by tables outward from the singularity for a small distance, beyond which numerical integration is employed. The singularity at F results in an indeterminate value for the integrand. Numerical integration can be carried across this singularity, however, as the application of L'Hospital's rule yields a finite value for the integrand at F.

Points A, D and H, which lie at infinity in the z plane, require careful consideration in the numerical integration. In all three cases integration was carried out towards the singularity until uniform flow was approximately attained, at which location the velocity potential is a straight line. Imposing this criterion allowed calculation of the change in the x and y co-ordinates between points C and E, G and I, and B and J, the last of which provided a confirmation of the solution.

We obtain the jet angles δ_D and δ_H from (2) and (28). At D

$$\delta_D = \pi(\phi_{1F} - \tfrac{1}{2}) + \mathrm{Im}\,[\tfrac{1}{2}\ln F_4(iK\psi_{1D}) + \ln F_5(iK\psi_{1D})]. \tag{37}$$

If b_1 and b_2 are defined as the straight-line distances between C and E, and G and I, respectively, it can be shown that the ratios of jet width to channel width are

$$\frac{C_{c1}b_1}{B} = \frac{(t_F - t_H)(t_A - t_D)}{(t_F - t_A)(t_H - t_D)}\frac{V_0}{U}, \tag{38}$$

$$\frac{C_{c2}b_2}{B} = \frac{(t_F - t_D)(t_H - t_A)}{(t_F - t_A)(t_H - t_D)}\frac{V_0}{U}, \tag{39}$$

where C_{c1} and C_{c2} are the corresponding coefficients of contraction. Equations (38) and (39) together satisfy continuity:

$$\frac{C_{c1}b_1}{B} + \frac{C_{c2}b_2}{B} = \frac{V_0}{U}. \tag{40}$$

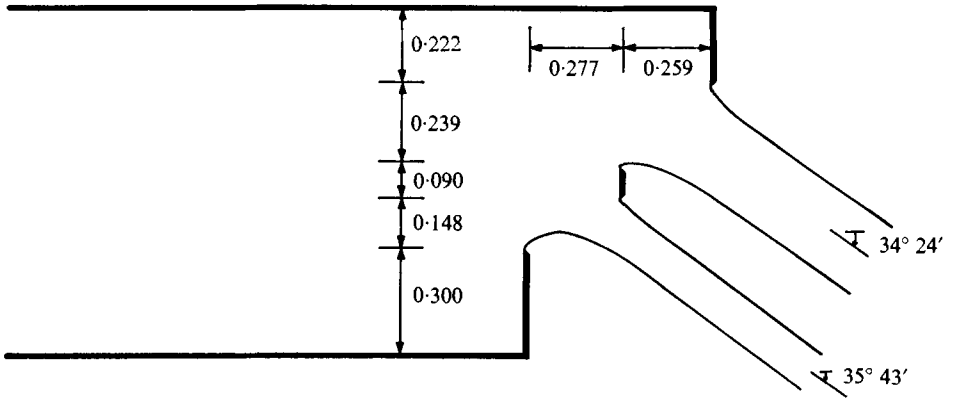

FIGURE 5. Solution for $k^2 = 0{\cdot}5$, $\phi_{1B} = 0{\cdot}2$, $\phi_{1A} = 0{\cdot}7$, $\phi_{1J} = 0{\cdot}8$, $\psi_{1D} = 0{\cdot}2$, and $\psi_{1H} = 0{\cdot}7$. Dimensions in multiples of B.

The velocity ratio is evaluated from (28) as

$$V_0/U = \mathrm{Re}\,[\exp(\Omega_A)]. \tag{41}$$

The contraction coefficients are computed from (38) and (39) once the distances b_1 and b_2 have been determined by integration of (34). A complete integration of (34) along all nine lines in the w_1 plane yields the actual configuration in the z plane as well as b_1 and b_2, from which the contraction coefficients can be calculated.

We obtained the pressure distribution on the end plates BC, EG and IJ from (2), (28) and Bernoulli's equation. By independent evaluation of the total force on all three end plates from momentum analysis and from numerical integration of the pressure distribution, the solution was confirmed.

An arbitrary selection of values of ψ_{1D}, ψ_{1H}, ϕ_{1A}, ϕ_{1B} and ϕ_{1J} for a given k^2 will yield an asymmetric configuration, for which the end plates will in general not be lined up. The results of one particular selection of parameters is shown in figure 5. For parametric studies of more general configurations than the symmetric two-jet (asymmetric single-jet) problem reported in § 5, relationships among the six quantities above must be established in order to investigate two asymmetric jets with all three plates in line.

A two-jet problem with complete symmetry about F is possible only if $\psi_{1D} = \psi_{1H}$, $\phi_{1A} = \phi_{1F} = \frac{1}{2}$, and $\phi_{1J} = 1 - \phi_{1B}$. If these constraints are applied, end plates BC and IJ line up but the middle plate EG is not in general in the same plane as the other two.

5. Asymmetric single jet

The single-jet problem discussed by Cisotti (1908), Greenhill (1910) and Michell (1890) can be effected by imposing complete symmetry about F. For a given k^2, only ϕ_{1B} and ψ_{1D} can be chosen arbitrarily. The particular solution for which the two end plates are in line, as shown in figure 6, will be determined. Furthermore, values of the jet angle and coefficient of contraction are sought for particular values of the ratio b/B of slot width to channel width.

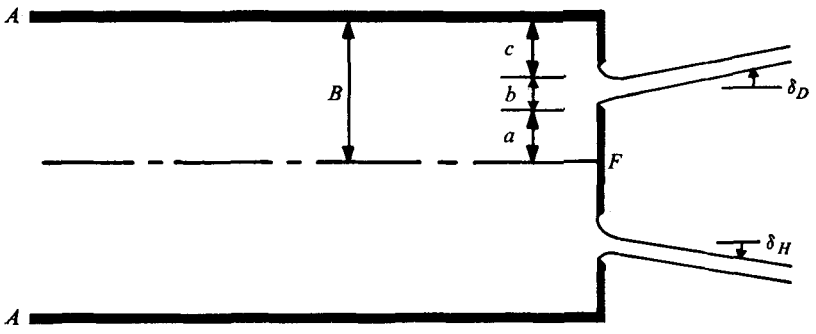

FIGURE 6. Definition sketch for single-jet configuration.

a/B	C_c	δ_D
	$b/B = 0{\cdot}1$	
0·8984	0·643	15° 5′
0·896	0·636	13° 23′
0·892	0·631	11° 44′
0·886	0·626	10° 7′
0·877	0·622	8° 27′
0·862	0·618	6° 39′
0.826	0·615	4° 25′
0·600	0·6124	0° 54′
	$b/B = 0{\cdot}4$	
0·5988	0·682	17° 44′
0·595	0·671	15° 48′
0·588	0·662	13° 59′
0·579	0·654	12° 14′
0·565	0·648	10° 31′
0·542	0·643	8° 45′
0·515	0·639	6° 54′
0·466	0·635	4° 45′
0·369	0·6319	1° 45′
	$b/B = 0{\cdot}7$	
0·297	0·736	14° 26′
0·293	0·723	12° 35′
0·283	0·712	10° 44′
0·270	0·704	8° 52′
0·251	0·697	6° 55′
0·186	0·688	2° 13′
0·171	0·6871	1° 15′

a/B	C_c	δ_D
	$b/B = 0{\cdot}2$	
0·7977	0·655	16° 41′
0·794	0·647	14° 52′
0·789	0·640	13° 10′
0·781	0·634	11° 31′
0·770	0·629	9° 52′
0·753	0·625	8° 10′
0·725	0·621	6° 18′
0·661	0·618	3° 58′
0·629	0·6173	3° 13′
0·578	0·6166	2° 17′
0·463	0·6159	0° 35′
	$b/B = 0{\cdot}5$	
0·486	0·674	13° 15′
0·458	0·660	9° 41′
0·401	0·650	5° 50′
0·360	0·647	3° 56′
0·347	0·646	3° 26′
0·300	0·6449	1° 41′
0·256	0·6445	0° 12′
	$b/B = 0{\cdot}8$	
0·1981	0·767	12° 21′
0·193	0·754	10° 31′
0·183	0·743	8° 38′
0·169	0·735	6° 39′
0·150	0·728	4° 29′
0·123	0·723	2° 0′
0·114	0·7228	1° 13′

a/B	C_c	δ_D
	$b/B = 0{\cdot}3$	
0·6992	0·672	18° 17′
0·696	0·662	16° 20′
0·691	0·653	14° 31′
0·683	0·646	12° 48′
0·672	0·640	11° 7′
0·657	0·635	9° 25′
0·633	0·630	7° 39′
0·593	0·627	5° 41′
0·508	0·6235	3° 5′
0·467	0·6229	2° 11′
0·406	0·6223	1° 1′
	$b/B = 0{\cdot}6$	
0·3983	0·712	15° 55′
0·393	0·700	14° 1′
0·384	0·690	13° 12′
0·372	0·682	10° 23′
0·354	0·676	8° 32′
0·328	0·670	6° 33′
0·291	0·666	4° 17′
0·235	0·6626	1° 34′
	$b/B = 0{\cdot}9$	
0·0984	0·817	9° 0′
0·093	0·803	7° 9′
0·084	0·792	5° 9′
0·074	0·786	3°32′
0·070	0·784	2° 53′
0·052	0·7806	0° 12′

TABLE 1. Calculated coefficient of contraction and deflexion angle for asymmetric single jet.

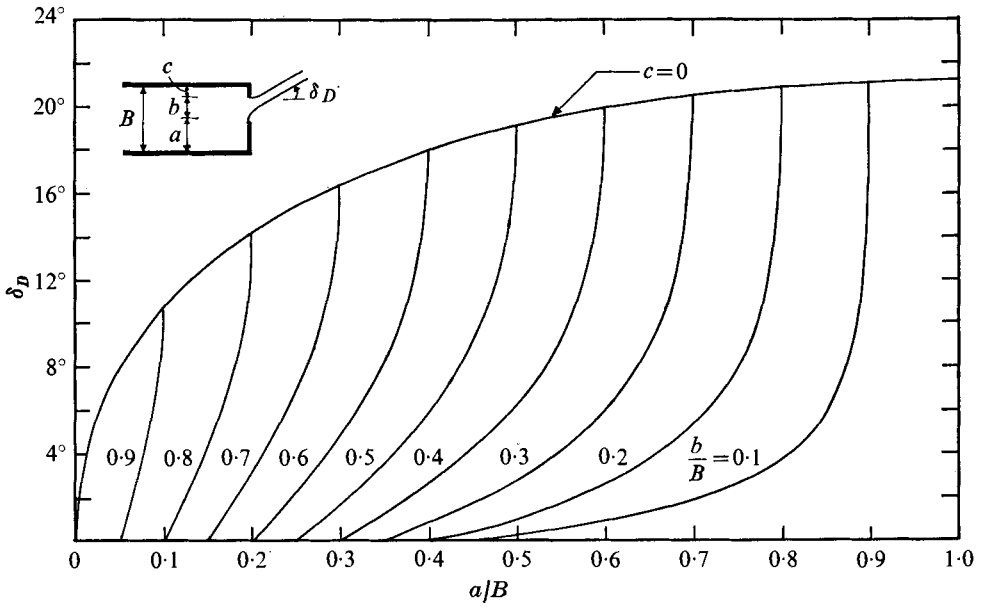

FIGURE 7. Deflexion angle for single jet.

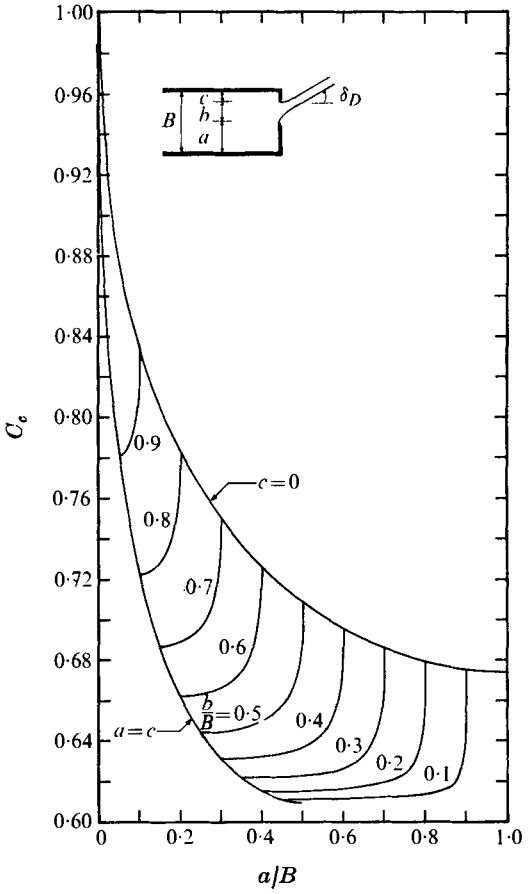

FIGURE 8. Coefficient of contraction for single jet.

	Symmetric slot ($a = c$)		*Asymmetric slot* ($c = 0$)			
	C_c		C_c		δ_D	
b/B	von Mises	Martin	von Mises	Martin	von Mises	Martin
0·0	0·611	0·6110	0·673	0·6744	21° 0′	21° 8′
0·1	0·612	0·6122	0·676	0·6757	20° 55′	21° 3′
0·2	0·616	0·6158	0·680	0·6795	20° 35′	20° 50′
0·3	0·622	0·6221	0·686	0·6862	20° 5′	20° 26′
0·4	0·633	0·6314	0·693	0·6959	19° 40′	19° 51′
0·5	0·644	0·6444	0·702	0·7092	19° 0′	19° 1′
0·6	0·662	0·6621	0·720	0·7270	18° 0′	17° 54′
0·7	0·687	0·6867	0·740	0·7509	16° 30′	16° 22′
0·8	0·722	0·7223	0·782	0·7840	14° 20′	14° 10′
0·9	0·781	0·7806	0·842	0·8347	11° 5′	10° 44′

TABLE 2. Comparison of particular solutions of present study with those of von Mises.

By specifying k^2 and ϕ_{1B}, values of ψ_{1D} for $\Delta x_{CE} = 0$ were obtained by interpolating for ψ_{1D}. The functional relationship between ψ_{1D} and ϕ_{1B} was established under the condition $\Delta x_{CE} = 0$. For this relationship corresponding values of b/B as a function of ϕ_{1B} were determined. Parabolic interpolation techniques were employed to define the functional relationships b/B *vs.* ϕ_{1B} and ψ_{1D} *vs.* ϕ_{1B}. For $b/B = 0{\cdot}1(0{\cdot}1)0{\cdot}9$ values of ϕ_{1B} and ψ_{1D} were obtained by parabolic interpolation. Usually the integration of (34) resulted in $\Delta x_{CE} = 0$, with b/B as specified. If not, another cycle of interpolation and integration was performed. The total force on all three end plates calculated from an integration of the pressure distribution never differed by more than 0·05 % from that based upon momentum principles.

The coefficient of contraction of the jet C_c and the angle of deflexion δ_D are given in table 1. The angle of the jet is negative for small values of k^2 but becomes positive as k^2 approaches unity. For a given value of b/B identical results were obtained for negative and positive jet deflexion angles if a/B and c/B were equal. Physically, the two symmetric jets would of course intersect for negative values of δ_D. The implication of jet intersection and the question of simply connected regions will not be discussed in the paper. All values listed in table 1 correspond to positive values of δ_D, however.

Figure 7 shows the dependence of δ_D on a/B for various values of b/B. The two limiting cases are the von Mises symmetric single jet ($\delta_D = 0$) and the von Mises asymmetric single jet for which $c/B = 0$. The latter solution is represented by the upper curve. The coefficient of contraction is depicted in figure 8 in terms of a/B and b/B also. In this figure the upper curve represents the asymmetric jet and the lower curve the symmetric one. Separate solutions were obtained for the two limiting cases to provide confirmation of the more general solution, and to improve the accuracy of the original values reported by von Mises (1917) and later by Robertson (1965, p. 512). We list the results of these particular solutions along with the original values reported by von Mises in table 2. For the symmetric slot ($b/B = 0{\cdot}4$) the value of C_c has been reported by von Mises as 0·633, by Rouse (1946, p. 57) as 0·631 and by Robertson (1965) as 0·632. In the case of the

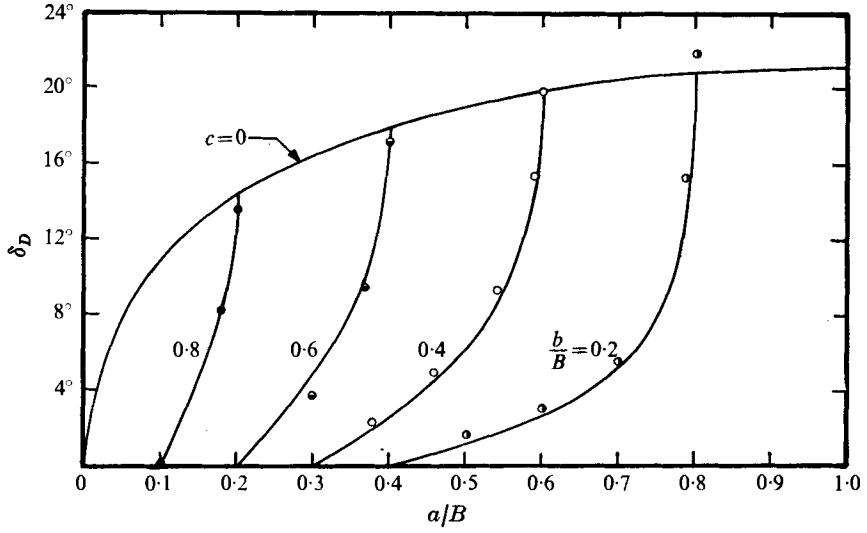

FIGURE 9. Comparison of theoretical and experimental deflexion angles. Measured points from Chowchuvech: ◑, $b/B = 0{\cdot}2$; ○, $b/B = 0.4$; ◒, $b/B = 0.6$; ●, $b/B = 0.8$.

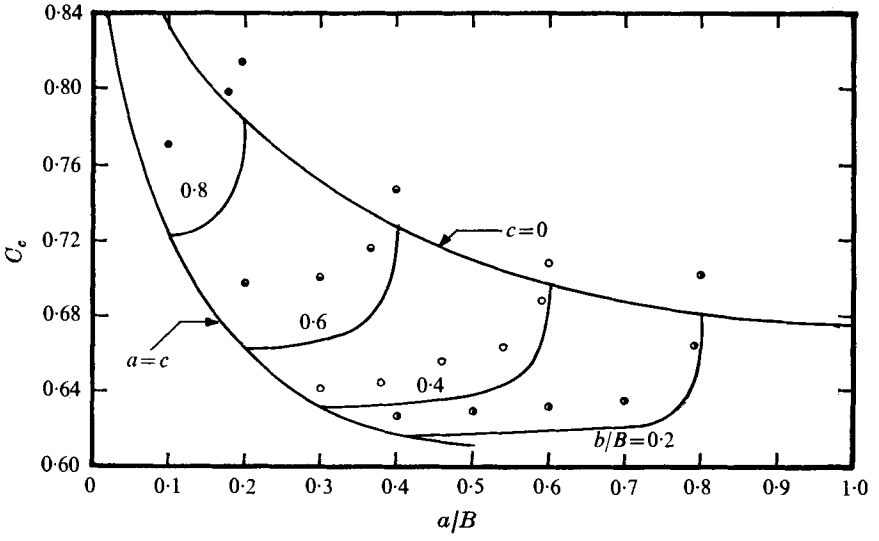

FIGURE 10. Comparison of theoretical and experimental coefficients of contraction. Measured points from Chowchuvech: ◑, $b/B = 0{\cdot}2$; ○, $b/B = 0{\cdot}4$; ◒, $b/B = 0{\cdot}6$; ●, $b/B = 0{\cdot}8$.

asymmetric slot the variance is considerably greater for a number of values of b/B.

6. Comparison with experiment

For the asymmetric single-jet problem experimental results are available. Chowchuvech (1961) measured the deflexion angle and the coefficient of contraction of a water jet discharging into the atmosphere through a rectangular channel

2·54 cm high and 10·16 cm long. By means of two end plates the horizontal dimension was reduced in order to vary a/B over a range of values for $b/B = 0{\cdot}2$, 0·4, 0·6 and 0·8. The effect of gravity on the flow upstream and downstream of the orifice was minimized, if not eliminated, by maintaining quite high Froude numbers.

A comparison of the measured jet deflexion angles with the theoretical ones is shown in figure 9. Good agreement is obtained primarily because the angle that the jet attains is basically influenced by momentum considerations, which are easily represented in this simple accelerated flow. On the other hand, the comparison of the measured and theoretical coefficients of contraction shown in figure 10 is not nearly as favourable. In this instance the discrepancy may be caused by surface-tension effects for the initially rectangular jet. The measured values of C_c are frequently greater than the theoretical ones, as was found by Weisbach (Birkhoff & Zarantonello 1957, p. 33), for a symmetric jet issuing from a rectangular slot.

This investigation was supported in part by the National Aeronautics and Space Administration under Grant NGR-11-002-033. The computational facilities provided by Professor E. Naudascher, Institute of Hydromechanics, University of Karlsruhe, Germany, are acknowledged. The author is also indebted to the helpful suggestions of Professor T. Sarpkaya, Naval Postgraduate School, Monterey, California.

Appendix

The Jacobian elliptic functions are related to the theta functions as follows:

$$\operatorname{sn} u = \frac{H(u)}{k^{\frac{1}{2}}\Theta(u)}, \quad \operatorname{cn} u = \left(\frac{k'}{k}\right)^{\frac{1}{2}} \frac{H_1(u)}{\Theta(u)}, \quad \operatorname{dn} u = k'^{\frac{1}{2}} \frac{\Theta_1(u)}{\Theta(u)}. \quad (42), (43), (44)$$

If q is Jacobi's *nome* the four theta functions can be expanded in rapidly converging Fourier series (Byrd & Friedman 1954, p. 314):

$$\Theta(u) = 1 + 2 \sum_{n=1}^{\infty} (-1)^n q^{n^2} \cos\left(\frac{n\pi u}{K}\right), \quad (45)$$

$$H(u) = 2 \sum_{n=1}^{\infty} (-1)^{n-1} q^{(n-\frac{1}{2})^2} \sin\left((2n-1)\frac{\pi u}{2K}\right), \quad (46)$$

$$H_1(u) = 2 \sum_{n=1}^{\infty} q^{(n-\frac{1}{2})^2} \cos\left((2n-1)\frac{\pi u}{2K}\right), \quad (47)$$

$$\Theta_1(u) = 1 + 2 \sum_{n=1}^{\infty} q^{n^2} \cos\left(\frac{n\pi u}{K}\right), \quad (48)$$

where u is a complex variable.

REFERENCES

ABRAMOWITZ, M. & STEGUN, I. A. 1964 *Handbook of Mathematical Functions*. Washington: Nat. Bur. Stand.

BIRKHOFF, G. & ZARANTONELLO, E. H. 1957 *Jets, Wakes and Cavities*, vol. 2. Academic.

BYRD, P. F. & FRIEDMAN, M. D. 1954 *Handbook of Elliptic Functions for Engineers and Physicists*. Springer.

CASSIDY, J. J. 1965 Irrotational flow over spillways of finite height. *J. Engng Mech. Div., Proc. A.S.C.E.* **91** (EM6), 155–173.

CHOWCHUVECH, S. 1961 Flow and discharge characteristics of a two-dimensional orifice (slot) placed unsymmetrically in the approach channel. M.S. thesis, SEATO Graduate School of Engineering.

CISOTTI, U. 1908 Vene fluenti. *Rendiconti del Circolo Matematico di Palermo*, **25**, 145–179.

CISOTTI, U. 1914 Efflusso da un recipiente forato lateralmente. *Rendiconti Reale Accademia dei Lincei, Roma*, **23**, 73–79.

GREENHILL, G. 1910 Theory of a streamline past a plane barrier. *Adv. Comm. Aero., Lond. R. & M.* no. 19.

JACOBI, C. G. J. 1881 *Gesammelte Werke*, vol. 1, p. 197. Berlin.

MARKLAND, E. 1965 Calculation of flow at a free overfall by relaxation method. *Proc. Inst. Civil Engrs*, **31**, 71–78.

MARTIN, C. S. 1967 Hydrodynamics of tire hydroplaning. *J. Aircraft, A.I.A.A.* **4**, 136–140.

MICHELL, J. H. 1890 On the theory of free streamlines. *Phil. Trans.* **81**, 389–431.

MISES, R. VON 1917 Berechnung von Ausfluss und Überfallzahlen. *Z. ver. dtsch. Ing.* **61**, 447–452, 469–473, 493–498.

ROBERTSON, J. M. 1965 *Hydrodynamics in Theory and Application*. Prentice-Hall.

ROUSE, H. 1946 *Elementary Mechanics of Fluids*. Wiley.

STRELKOFF, T. & MOAYERI, S. 1970 Pattern of potential flow in a free overfall. *J. Hydraul. Div. Proc. A.S.C.E.* **96** (HY4), 879–901.

THOM, A. & APELT, C. J. 1961 *Field Computations in Engineering and Physics*. Van Nostrand.